Characterization of space dust using acoustic impact detection

Robert D. Corsaro, Frank Giovane, Jer-Chyi Liou, Mark J. Burchell, Michael J. Cole, Earl G. Williams, Nicholas Lagakos, Albert Sadilek, and Christopher R. Anderson

Citation: The Journal of the Acoustical Society of America **140**, 1429 (2016); doi: 10.1121/1.4960782
View online: https://doi.org/10.1121/1.4960782
View Table of Contents: https://asa.scitation.org/toc/jas/140/2
Published by the Acoustical Society of America

Characterization of space dust using acoustic impact detection

Robert D. Corsaro[a)]
Sotera Defense Solutions, 7230 Lee DeForest Drive, Columbia, Maryland 21046, USA

Frank Giovane
Department of Physics, Virginia Polytechnic Institute, Blacksburg, Virginia 24060, USA

Jer-Chyi Liou
NASA Orbital Debris Program Office, NASA/JSC, Houston, Texas 77058, USA

Mark J. Burchell and Michael J. Cole
School of Physical Sciences, University of Kent, Canterbury, Kent CT2 7NH, United Kingdom

Earl G. Williams and Nicholas Lagakos[b)]
Naval Research Laboratory, Code 7130, Washington, D.C. 20375, USA

Albert Sadilek and Christopher R. Anderson
U.S. Naval Academy, Annapolis, Maryland 21402, USA

(Received 4 September 2015; revised 10 May 2016; accepted 21 May 2016; published online 31 August 2016)

This paper describes studies leading to the development of an acoustic instrument for measuring properties of micrometeoroids and other dust particles in space. The instrument uses a pair of easily penetrated membranes separated by a known distance. Sensors located on these films detect the transient acoustic signals produced by particle impacts. The arrival times of these signals at the sensor locations are used in a simple multilateration calculation to measure the impact coordinates on each film. Particle direction and speed are found using these impact coordinates and the known membrane separations. This ability to determine particle speed, direction, and time of impact provides the information needed to assign the particle's orbit and identify its likely origin. In many cases additional particle properties can be estimated from the signal amplitudes, including approximate diameter and (for small particles) some indication of composition/morphology. Two versions of this instrument were evaluated in this study. Fiber optic displacement sensors are found advantageous when very thin membranes can be maintained in tension (solar sails, lunar surface). Piezoelectric strain sensors are preferred for thicker films without tension (long duration free flyers). The latter was selected for an upcoming installation on the International Space Station.
[http://dx.doi.org/10.1121/1.4960782]

[TGL] Pages: 1429–1438

I. INTRODUCTION

Dust is a ubiquitous component of our galaxy and Solar System. The Earth accumulates roughly 100 tons of space dust each day. The term "dust" encompasses all solid particles in space smaller than 2 mm. Measurements of dust properties and its population distribution provide important information to space science in modeling the birth and growth of the Solar System. We will not attempt to review this broad and active field. There are excellent books available on this subject (e.g., Grun *et al.*, 2001) and frequent international conferences with published proceedings (e.g., Green *et al.*, 2002). The scope of this paper will be restricted to an overview of a recent set of studies using acoustic sensors, leading to a new instrument for measuring the flux and dynamics of dust particles in space.

The principle dust component of interest here are micrometeoroids (MM). These are usually defined as the largest of the interplanetary "dust" particles with diameters 50 μm to 2 mm. The majority of those encountered originate within the Solar System, typically from comets or as ejecta from planetary or asteroid surfaces following impacts. Other particles date to the birth of the Solar System and a small fraction are interstellar. These particles travel with hypersonic speeds typically in the range 10–70 km/s. Their distribution in space and their size-population relationship are non-uniform; space probes rarely encounter MM particles while impacts from small micron-size dust particles may be quite frequent. Space scientists are interested in characterizing this particle population for various reasons, among them because they provide an accessible sample of a distant astronomical body, are major contributors to the growth of planetary surfaces, and provide information about the origin and dynamics of the early Solar System.

MM particles do not survive intact during passage though the Earth's atmosphere. Hence, they must be measured in space or captured and retrieved. Since the beginning of the space age, impact detectors have been installed on spacecraft to determine the flux of the smaller dust particles. The history and variety of these impact detectors is extensive. One frequently used detector uses a polyvinylidene

[a)]Electronic mail: Bob@AstroAcoustics.com
[b)]Current address: Sotera Defense Solutions, Columbia, MD 21046, USA.

fluoride (PVDF) piezoelectric film as the impact target and detects the charge generated on the film from local impact-depolarization. This sensor has been used in various spacecraft including Argos (e.g., Tuzzolino *et al.*, 2005) and Stardust (e.g., Tuzzolino *et al.*, 2003). Other detectors use acoustic signals generated by lead zirconate titanate (PZT) piezoelectric sensors, both as impact plates and also as sensors attached to aluminum target plates. More common sensor technologies include charged capacitors, optical impact flash and particle charge detectors, laser curtains, and telescopic observation of reflected sunlight. There are also return missions where particles have been captured in aerogel such as Stardust and the EuReCa spacecraft (Burchell *et al.*, 1999b) or where population statistics are inferred by studying the damage to returned structures, such as parts retrieved from Hubble (Liou, 2013; Kearsley *et al.*, 2007). There are also numerous proposed techniques that have been partially developed but have not yet flown in space, and reviews of these appear elsewhere (e.g., Christiansen, 2009).

The information gained from studying these small particles has been valuable for improving our understanding of the ongoing physical processes of asteroids, comets, Kuiper Belt objects,and planetary rings. However, these instruments typically have one or both of the following limitations: they do not measure the dynamics of the particles and they are limited in size.

With few exceptions, the instruments that have flown only measure particle flux sorted by size. Since the speed, direction, and location are typically undetermined, the impacting particles cannot be traced back to an originating body (planetary surface, comet, region of space, etc.). This is a significant loss of potentially valuable information regarding the dynamics of our Solar System. There are also two special environments where measurement of particle dynamics is important to distinguish MM particles from other particulate contributors. The most frequently studied is near Earth, using instruments in orbit. Here, manmade orbital debris forms a second particle component. Data collected during the early space age are relatively uncontaminated (though limited), however, the debris population has progressively accumulated. In recent years it has increased dramatically, particularly at higher altitudes. The debris population (0.1 mm or larger) at 400 km altitude is currently comparable to that of MM particles, while at 800 km it is 100 times greater. There are important practical reasons for accurately characterizing this debris population (i.e., hazard assessment). However, here our interest is in identifying a procedure to distinguish and remove debris impacts from the data set. Measuring the speed and trajectory of the impacting particles provides the needed tool since debris is orbital while MM is not. The second environment of interest is the lunar surface, where there is the opportunity to deploy very large area detectors. An instrument located there would also detect impacts from secondary ejecta (SE). This dust component originates from a meteor impact on the surface, which then launches large quantities of ejecta to high altitudes. Much of this SE dust then falls back to the surface at relatively slow speeds (typically 50–300 m/s). An understanding of this dust population is important to understanding the growth process of regolith and the shaping of the planetary body. Since these SE particles travel at relatively low speeds, a measurement of particle speed would distinguish SE from the interplanetary dust population.

An instrument designed to characterize the MM population must also have a relatively large cross section. The previously used instruments, with few exceptions, have target areas less than $0.1\,m^2$. On average, a target $0.1\,m^2$ is impacted by only four particles per year larger than $20\,\mu m$ (Liou *et al.*, 2005). Hence, these small targets can develop reliable statistics only on the smaller dust particles. Particles in the MM size range ($50\,\mu m$–2 mm) are much less frequent and measurement of their flux requires a much larger aperture instrument. In our region of space (1 AU), the current estimate is that a $1\,m^2$ target area will be impacted by 10 to 40 particles larger than $50\,\mu m$ per year (Liou *et al.*, 2005). For larger particles, the flux decreases quickly. For example, to detect even one particle per year that is 0.5 mm or larger, the target would need to be 20–80 m^2.

The instrument discussed here was developed in response to gaps in our understanding of the MM particle population and the need for more comprehensive characterization of their properties and kinetics. Its objectives include measuring the speed, direction, and arrival time (which is keyed to location) of individual MM particles in deep space or in the environments mentioned above.

II. APPROACH

Figure 1 illustrates the instrument configuration considered here. The impact targets are membranes—thin polymer films adhered to support frameworks. While single membrane systems might be useful for flux measurements on missions of opportunity we concentrate here on systems with two membranes separated by a known distance. The membranes are thin enough that the particles of interest are not significantly slowed or disrupted on passing through the first membrane. The impact on each membrane generates acoustic signals that are detected by a set of sensors located near

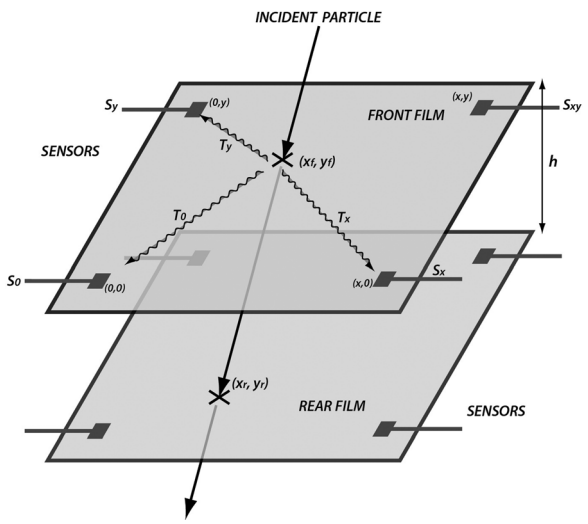

FIG. 1. Illustration of the instrument concept. Parameters shown are used in the Appendix.

the membrane edge. The signal arrival times at the set of sensors is then used in a multilateration calculation to identify the time and location of the impact on each membrane. Since the membrane separation distance is known, the difference in impact locations provides the particle direction. Particle speed is then calculated using the difference in impact times.

For space missions this dual-membrane configuration has a number of practical features. Since the target is a thin film, the overall mass can be very low. It can be configured to collapse for transport and be extended to a large area during deployment. Multiple units can also be easily stacked for transport and distributed to cover wider areas. Suitable membrane materials include Kapton and Mylar, which are readily available in thin films ranging from 2 to 100 μm. They have high tear strength, low creep, and are qualified for use in space.

From the above, it is clear that accurately identifying impact locations on each film is a key requirement. There are many multilateration algorithms commonly available but all use iterative techniques. Although these can rapidly converge to a solution, in processor-limited deployments these iterative techniques can be cumbersome to implement. For this application we derived a simple closed-form analytical expression that has been very successful. It makes use of two geometry constraints applicable to our systems: the surface is planar, and the sensors can be located orthogonally. The equations and derivation are summarized in the Appendix as they may find use in locating noise sources on quasi-planer surfaces in other acoustic applications.

The acoustic challenge then is to develop a sensor system capable of accurately measuring impact signals generated on large films by particles 50 μm in diameter or larger.

III. EXPLORATORY STUDIES

There are various design and configuration options that initially must be investigated. These include evaluating sensor types, determining if membrane tension is relevant or advantageous, and exploring the location-uniformity of the impact-sensor response function. For practical reasons, exploratory investigations of these factors use just a single membrane and subsonic particle impacts.

A. Sensor selection

Two sensor systems were considered and evaluated: a piezoelectric sensor, and a fiber optic sensor. Both have inherently high sensitivity, and low resource requirements (mass, power, cost). Both sensors and their associated systems can be fabricated using space-qualified components—an important requirement for a flight-ready instrument.

The piezoelectric sensor used is PVDF. Initially the PVDF sensors were used at the Naval Research Laboratory (NRL) for instrumenting an aerogel capture tray where it would record the time of micrometeoroids impacts and identify the particle location for analysis on tray retrieval (Corsaro *et al.*, 2004; McKee, 2004; Liou *et al.*, 2007). At the conclusion of that program the sensor system was reconfigured for impact damage detection on human habitats. This system performed well during two NASA desert exercises using mock lunar modules (Corsaro *et al.*, 2011; Opiela *et al.*, 2011). For the current application on thin films, these sensors have desirable properties: they are small, flexible, thin, and have wide bandwidths with high sensitivity to in-plane strain. One initial concern was mechanical loading of the film by these sensors. For the studies reported here the typical sensor thickness used is 25 μm. These perform very well on 25 μm and thicker films, and retained acceptable (though reduced) sensitivity on all thinner films studied, including even the 2-μm thick membrane. The sensors themselves require no electrical power although the associated system electronics does. They retain good sensitivity at cryogenic temperatures and, when fabricated using an elevated annealing temperature, they withstand temperatures to +120 °C.

The fiber optic displacement (FOD) sensor system was initially developed at NRL for general acoustic studies (Bucaro *et al.*, 2005; Lakagos *et al.*, 2012). It is a non-contact surface-normal displacement sensor using the intensity of reflected incoherent light. It consists of an optical fiber bundle, with the central fiber illuminated by a light emitting diode (LED). Light travels down this fiber and exits at the target end as a cone of light that is reflected by the target surface. The reflected light illuminates the outer fibers and is returned to a photo-detector where the intensity is measured. The reflected optical intensity varies with separation distance. At close distances it increases with separation distance since the reflected source cone progressively extends to include more of the sensor fibers area. In this region it has better than one angstrom distance resolution. Beyond some maximum distance (i.e., 0.6 mm) it decreases with distance as the source cone spreads beyond the radius of the detector fiber bundle. In this region the sensitivity is reduced, typically by a factor of ten, but it can then monitor larger displacements (several millimeters). Being an all-glass probe system FOD sensors have advantages in severe environments (temperature, radiation, etc.). The power requirements are modest, with the LED using the largest portion.

An additional sensor candidate was also studied but was found to offer no advantages. This sensor was a full membrane fabricated from a single sheet of metalized piezoelectric PVDF film, such that the entire membrane served as a sensor. The sensor performed well in impact tests, but was found to have approximately one tenth the sensitivity of the smaller PVDF sensors adhered to a Mylar film. This is attributed to two factors: strain averaging over the large sensor surface, and the larger sensor capacitance. It is not considered further here.

B. Subsonic impact tests with tensioned membranes

The importance of film tension is studied using relatively slow particle impacts on a membrane test-bed. The use of slow speeds in these initial studies was necessitated by the relatively high cost of hypervelocity shots. The device used in our initial tests is shown in Fig. 2. It consists of an aluminized Mylar sheet clamped to an outer ring. An inner circular ring is tensioned against this film using six compression springs

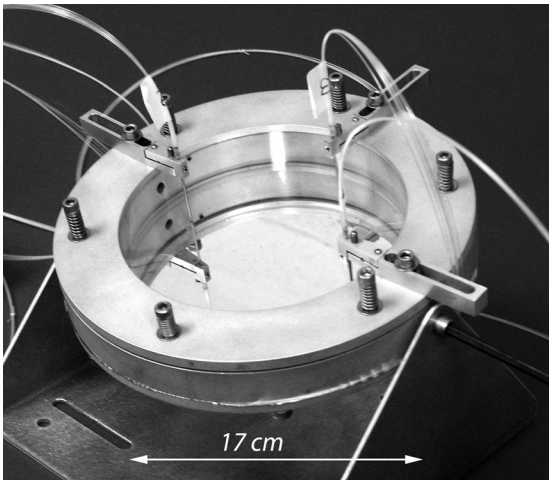

FIG. 2. The initial membrane impact test system. Rear view shows the three FOD sensors mounted on support arms and the six tensioning screws with springs.

surrounding the six tension adjustment screws. The diameter of the film for this test article is 17 cm (to fit in an available test chamber). Three PVDF sensors are attached to the membrane near the circumference. Three FOD sensors are attached to the support rim on the rear side of the unit. These FOD sensors can be positioned at any desired separation distance and location on the film, but typically are located 1 cm inward from edge and at a separation distance nominally 1 mm from the aluminized film.

The slow-speed tests were exploratory. In this speed regime the particle simply bounces off the surface without apparent damage. Since there was no penetration, these studies used only a single membrane. Figure 3 shows the signal amplitudes recorded for impacts from a range of particle masses and drop heights. The results shown used the FOD sensors, but data using the PVDF sensors are very similar. For all particles smaller than 50 g the signal amplitude appears directly proportional to momentum. The spectra are dominated by a series of maxima corresponding to (at least

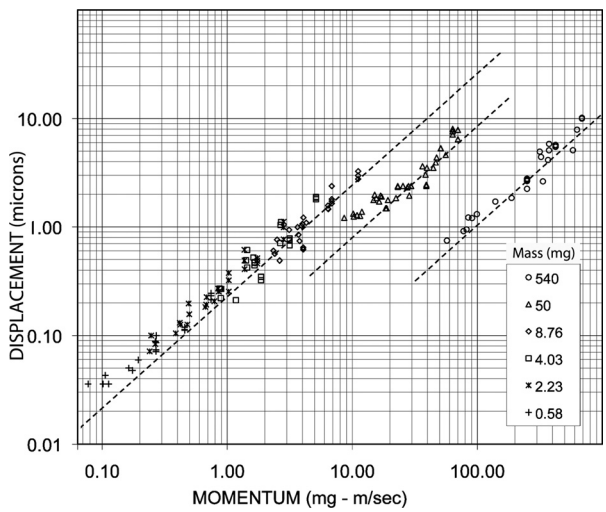

FIG. 3. Signal amplitude as a function of particle momentum for various diameter particles. Optical sensor data for slow-speed impacts are shown, but PVDF sensor data are similar. Legend shows particle mass in mg.

the first seven) symmetric modes of a circular membrane fixed at the rim and having a tension of ~211 N. The spectra show relatively uniform peak amplitude for all modes except the lowest (0,1). This lowest mode is not strongly excited by an impact at the location used.

The data for the two largest particles show the same slope but the fit appears translated down to lower signal voltages—that is, the motion at the sensor location on the membrane is smaller than expected but shows the same linear dependence on speed. The spectra again are dominated by a series of maxima corresponding to symmetric modes but now there is a significant decrease in the membrane response for the higher modes.

While the field of impact physics is extensive, Courbin *et al.* (2006) provides some relevant guidance on mechanisms involved. Non-penetrating membrane impacts are divided into four regions, divided by the values of two parameters. (A) The first includes a ratio of the particle speed to a term containing film tension and material modulus. All tests considered in this section used slow particle speeds, placing them in the regime where the acoustic response is controlled by the film tension rather than plate-like local deformation. (B) The second divider involves a parameter that includes a ratio of the particle mass to membrane mass. This ratio is small for most of the particles used in this study. Hence impacts from most of the particles launch acoustic membrane waves that are not influenced by the edge constraints, However, the two more massive particles used in this study approach a regime where the wave motion involves the entire membrane and begins to be controlled by the frame size. While these differences in behavior are interesting, this discussion can be deferred. For the application considered, the only environment where we might encounter large millimeter size particles traveling at slow speeds is on the lunar surface.

These tests were extended to include different frames and conditions. Studies included frame sizes from 0.17 to 1.0 m diameter and film tensions from 0 to 2.7 N. The system behaviors were similar, albeit the model frequencies were different. Higher particle impact speeds to 350 m/s were also studied using pressurized air rifles with particles 0.3–2 mm diameter. These higher speed impacts were often inelastic, producing significant surface damage. Signals were large but smaller than projected from the linear extrapolation of the slower speed data. This mid-speed region was not studied in detail, as it is not relevant to the application.

One significant observation in these studies is that the preferred sensor type depends on the tension in the film. For films with tension, the fiber optic sensor system more clearly measured the vibration modes while providing good sensitivity to transient acoustic arrivals and lower background noise. This excellent performance is due in part to the high sensitivity to surface displacement and its broad frequency bandwidth of DC to 1 MHz. However, for loosely held films with little or no tension, the film displacement can become large enough to exceed the measurement range of the optical sensor. In these cases the PVDF sensor performs better. This sensor responds to in-plane strain making it less sensitive to simple displacement and low frequency vibrational modes.

In part, this is because the sensor inherently contains a weak high-pass filter: the sensors equivalent circuit is a charge generator in parallel with a capacitor and resistor.

C. Response uniformity

One early concern was that on tensioned films the signal amplitude might vary considerably depending on the location of the impact. In tests on various films, we found no large amplitude changes as the impact location was changed. To improve our understanding of this we performed a numerical study of the influence of sensor and impact locations on the signal amplitudes detected. The governing equation in the time domain for the impulse response of a membrane excited at $t=\tau$ of strength $F\delta(\theta-\theta')\delta(r-\rho)/r$ is (Duffy, 2001)

$$g(r,\theta,t|\rho,\theta',\tau) = F\frac{c^2}{\pi a^2}e^{-b(t-\tau)}H(t-\tau)\sum_{m=0}^{\infty}\sum_{n=0}^{\infty}\varepsilon_m \times\frac{J_m(k_{nm}\rho/a)J_m(k_{nm}r/a)}{J_{m+1}^2(k_{nm})}\cos[m(\theta-\theta')] \times\frac{\sin\left[(t-\tau)\sqrt{c^2k_{nm}^2/a^2-b^2}\right]}{\sqrt{c^2k_{nm}^2/a^2-b^2}}, \quad (1)$$

where b is related to the damping of the membrane and $r=a$ is the boundary, k_{nm} the zeros given by $J_m(k_{mn})=0$, and $H(t-\tau)$ is the Heaviside step function. The response g corresponds to a unit force impacting the membrane at the point (ρ,θ'). If we set the damping to zero then the resonance frequencies of the membrane are given by $f_{nm}=k_{nm}c/(2\pi a)$. Assume measurements are made at a set of points (r_i,θ_i), where $1<i<Q$ and where Q is the number of receivers. The measured response is then, using Eq. (1), due to an impact at ρ,θ' and at time $\tau=0$ is

$$g(r,\theta,t|\rho,\theta',0) = F\frac{c}{\pi a}H(t)\sum_{m=0}^{\infty}\sum_{n=0}^{\infty}\varepsilon_m\sin(2\pi f_{nm}t) \times\frac{J_m(k_{nm}\rho/a)}{k_{nm}J_{m+1}^2(k_{nm})} \times J_m(k_{nm}r/a)\cos[m(\theta-\theta')]. \quad (2)$$

The result of this analysis is shown in Fig. 4 for four sensors locations ranging from the film center ($r=0$) to very near the edge ($r=0.95$). The spatial map is the relative sensor response as a function of impact location. In all cases the response is greatest when the impact is near the probe, but there is also some enhancement at the image point on the opposite side. The double peak for $r=0.5$ is a whispering gallery effect where there is symmetric response or image on the opposite side of the membrane from the impact point.

This analysis provides guidance on the variability of signal amplitude with impact location for tensioned membranes. For sensors mounted near the circumference ($r>0.7$) the response is typically within 3 dB of the average, which is considered adequate for our application. The important exception is the much higher response that occurs when the impact occurs near the sensor. As mentioned in the Appendix, this is unimportant in this application since any practical implementation would place a shield covering the small area around each probe to protect it from impacts.

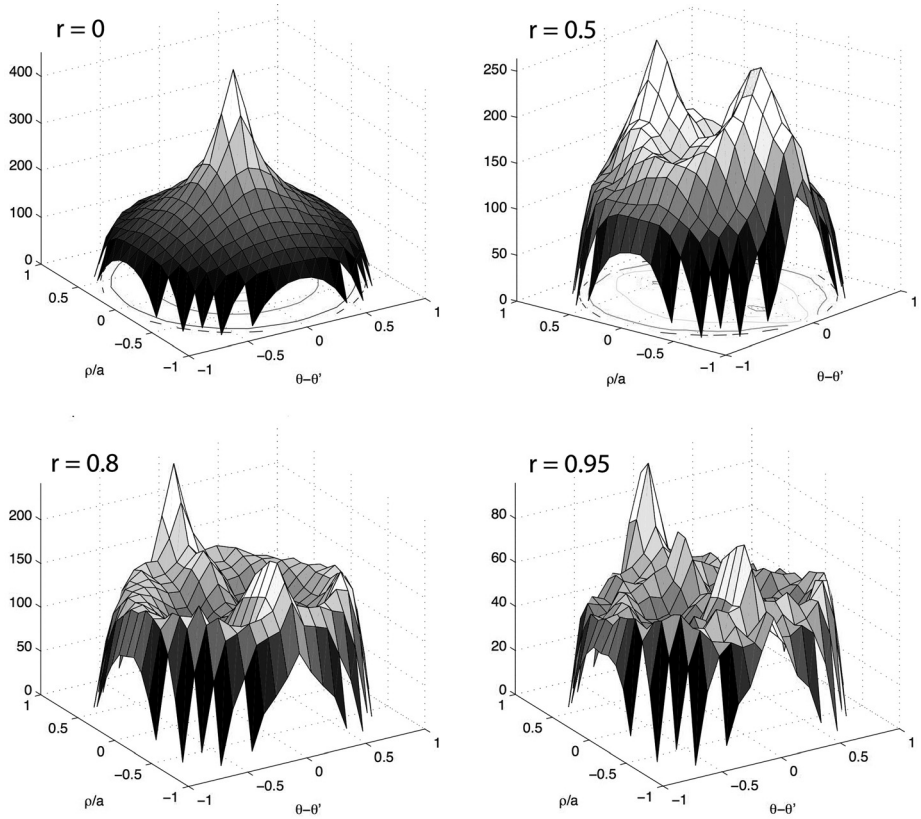

FIG. 4. Four examples of numerical model results. Each graph maps the relative surface displacement of a circular membrane for an impact at the designated location. Locations are relative to the membrane radius and range from film center ($r=0$) to very near the edge ($r=0.95$). Due to the symmetry of the equations, each can also be viewed as the relative response of a displacement sensor at the designated observation point mapped as a function of impact location.

IV. HYPERVELOCITY IMPACT TESTS

Once sufficient data and understanding were available for the subsonic particle impacts, the study was extended to explore instrument capability using hypervelocity impacts. All hypervelocity tests reported here are performed using the two-stage light-gas gun at the University of Kent at Canterbury, UK (Burchell *et al.*, 1999a). This facility can accommodate 1 m size targets and uses impact speeds of nominally 1–7.5 km/s, where speed is measured as the particle traverses between two light curtains. A four-section sabot is used to hold the particle, where the sabot is centrifugally separated from the particle during flight.

The particles used in the tests reported here had diameters much larger than the thickness of the film. They penetrated the material leaving holes only slightly (<10%) larger than their diameter. The sensor signals are typically large. They contain at least two components: an initial high-frequency signal corresponding to the impact transient (typically centered in the 40–70 kHz range) and a low frequency resonance with a dominant frequency f_0 that is typically below 10 kHz and influenced by the dimensions and properties of the sample.

The objective of this series of experiments is to compare the performance of the FOD and PVDF sensors. The low speed measurements found that the FOD sensors are best suited to membranes in tension, while the PVDF sensors are preferred on un-tensioned films. The hypervelocity experiments are designed to determine if either or both could measure the timing of the acoustic signals from a dual-membrane arrangement with sufficient accuracy to use it to determine particle impact location, speed and trajectory.

A. Film in tension

For applications where applying film tension is practical, it is desirable to used very thin films. The initial hypervelocity test used dual circular membranes fabricated from 4 μm aluminized Mylar film. These films were placed under tension using concentric hoops with tensioning bolts, similar to that used to tension drums, as shown in Fig. 5. Three FOD and three PVDF sensors were installed on each membrane to compare their characteristics. The membranes are 0.48 m in diameter and separated by 0.28 m. The fundamental frequencies indicate the tension on each film is nominally 6.3 N/m. Initial shots use 1 mm stainless steel balls travelling at nominally 5 km/s and 30° from membrane perpendicular. Sensor outputs were simultaneously captured with a 16-bit ADC at a sample rate of 1 MS/s per channel.

Typical signals are shown in Fig. 6 where in this case a 10 kHz high-pass filter is used to suppress offsets and low-frequency structural vibrations. On this film, the signal amplitude and SNR is much larger for FOD than PVDF. This is in part because the PVDF sensor is six times thicker than the membrane film and hence the film strain is only partially transferred to it. The FOD signals also appear to be more distinct and less susceptible to extraneous signal components. This is presumably because the out-of-plane displacement is relatively large, while the in-plane strain signal is smaller and is more easily contaminated by extraneous facility noise such as that associated with the projectile launch mechanism. The only issue with the FOD signals is that the signal records contain some dead regions where the arrival of the carrier gas displaced the film a distance

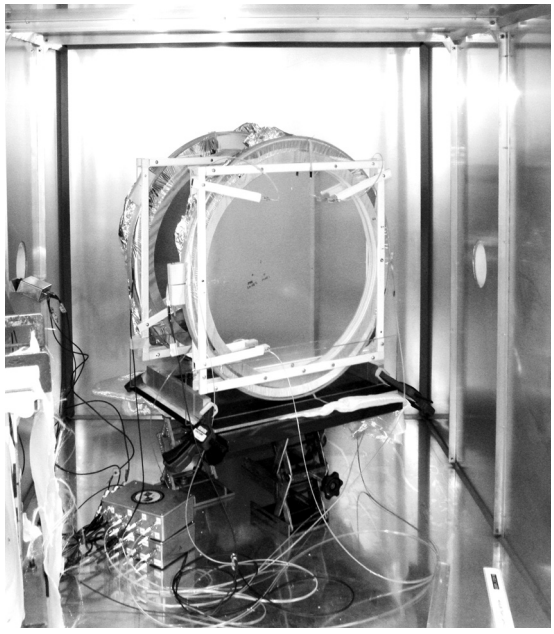

FIG. 5. Dual-drum assembly test article mounted in the hypervelocity impact chamber. Drum diameter is nominally 0.5 m and the impact chamber is a cube with 1.2 m sides.

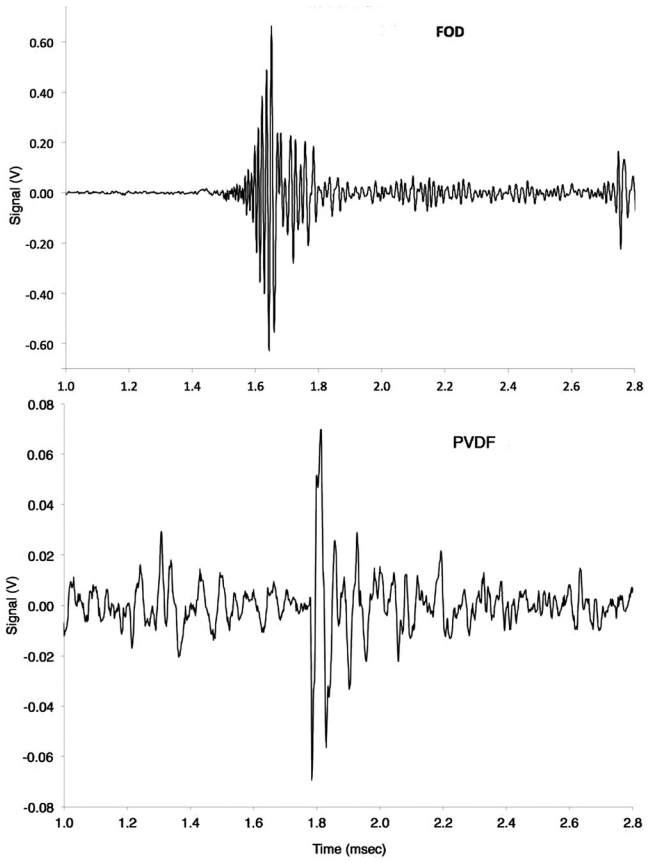

FIG. 6. Typical signals from the fiber optic (top) and PVDF sensors (bottom). Low frequency signals and offsets were removed using a 15 kHz high-pass filter.

exceeding the measurement range selected. This is an unavoidable facility artifact that would not exist in space.

The impact time and location results are found to be similar for both types of sensors. Both sets identified the impact location to within 3 cm, the particle speed to within ±2% and the direction to within 3°. Both also found the acoustic wave speed is nominally 122 m/s on this thin film. Repeat shots under various conditions showed similar results, but often with larger variations in the measured particle speed.

For this configuration using a very thin film in tension, the FOD sensor system performed better than PVDF. It does not load the surface and had higher sensitivity and lower signal attenuation. It is therefore the preferred sensor for very low mass films with very large target surfaces. In other tests it was also found to be more sensitive to small slow particles of the SE type present on the lunar surface. The drawbacks to the FOD sensor instrument include higher (though still small) electrical power requirements, and the need for maintaining film tension. Tension is difficult to maintain over long flight durations. However, there are special applications where it is relatively simple to implement, for example, in a gravity field (i.e., lunar or planetary surface) or as part of a solar sail (Corsaro *et al.*, 2007). The FOD sensor can also more easily measure modal frequencies, which could be useful in monitoring tension as well as identifying any film breakage.

B. Film without tension

In free-space it is more practical to use thicker films without tension. The results from the slow speed impact tests indicate that the PVDF sensor system is preferable in this case. The test article we initially used to study this configuration in hypervelocity studies consists of two Kapton films each 25 μm thick loosely adhered to a square 0.5×0.5 m frame. These two frames are separated by 15 cm. Four PVDF sensors are attached near the corners of each film. The low frequency vibrational signal is usually uninteresting and accompanied by noise in these tests, and is suppressed by a four-pole 15 kHz high-pass filter contained in the preamplifier.

This test article was used in a set of hypervelocity impact tests that included varying impact angle, speed, and particle diameter. The only *a priori* information used in the data analysis is the target geometry: the known locations of the sensors on each layer and the layer separation distance. The wave speed on these films was 1600 m/s ± 10% from previous measurements using known impact locations. This speed value depends on the type of Kapton film material and (because of dispersion) the frequency characteristics of the measuring system. The signal arrival times at each sensor were measured using a procedure that can be automated even in cases where there is minimal processing power available. It involves collecting the sensor acoustic signals, squaring them, and then creating a running summation. This forms a function related to cumulative signal energy arrival. The effective arrival time is then selected as the time where this function crosses some threshold value, such as 10% of the magnitude at the end of the signal record. From these arrival times, the impact locations are determined using the multilateration equation presented in the Appendix.

Figure 7 shows the resulting accuracy of the system in measuring impact location. This figure graphs the difference between the actual and calculated x,y-coordinates, where the actual locations are from observed impact holes and the calculated locations are from the acoustic arrival times. The average deviations are 1.4 cm for the front layer and 2.1 cm for the rear layer. While higher accuracy is desirable, these uncertainties are acceptable for the current application.

The particle direction is obtained using these impact coordinates. The results show an average deviation of 4°. With this trajectory and the known film separation distance, the path length that the particle traveled between the layers is calculated, and the particle speed can then be obtained using the measured impact times. These speeds can be compared to values measured by the facility's laser system. The results are in good agreement with an average error of only 13%. This accuracy is a function of the film separation distance used, as the speed measured for slow particles have higher accuracy due to their longer transit times between layers.

The signal levels decrease with travel distance due to geometrical spreading and dispersion. In this study, we find the cylindrical spreading loss is dominant. The additional attenuation is approximately 10 dB/m on the films used. This is used to adjust all signal levels to a reference travel distance (i.e., 0.25 m).

In a series of tests using a range of particle diameters (50–1000 μm), speeds (1–7 km/s), and angles (0–70°), the signal amplitudes on the forward film appear approximately proportional to the circumference of the hole produced. This relationship continues to be studied to determine its range of applicability, and two physics-based candidate mechanisms are being tested. At present, it is only claimed that the system is demonstrably capable of providing rough estimates of particle diameter from measured signal amplitude for most of the materials tested.

In some cases it is also possible to glean some information about the likely particle material. When using steel particles

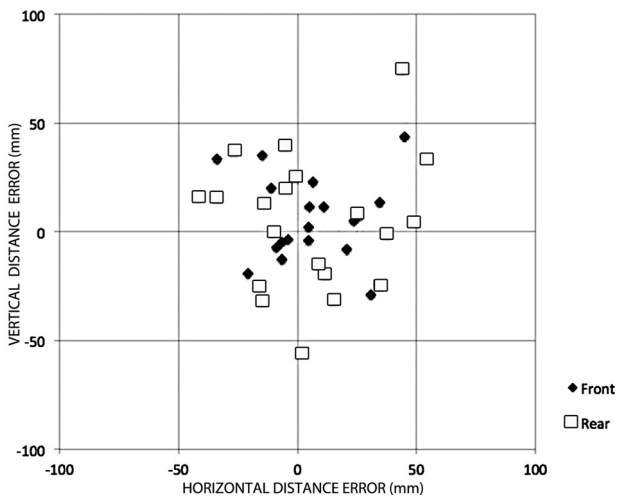

FIG. 7. Impact location measurement errors found using the acoustic system in various hypervelocity particle impact tests. Both front and rear membrane data are shown.

the signal amplitudes on the second film are typically five times larger than those on the first, due primarily to accumulated ejecta from the hole produced in the first film. However, when other materials are used (i.e., aluminum, copper, glass) the signal levels on the second layer are often comparable to or smaller than those on the first. In these cases, the particles are observed to have fractured on passing through the first layer. Some small particles (plastic and small non-ferrous) do not penetrate the first layer and thus produce no signals on the second. This suggests that for some impacts the ratio of the signal amplitudes on the two (or more) layers might be useful in distinguishing material type or morphology.

V. DISCUSSION

We examined the capability and limitations of dual-membrane impact targets instrumented with fiber optic and piezoelectric sensors. The study finds that this type of instrument is well suited for characterizing MM particles in space. The instrumented membrane has ample sensitivity for this application, and the dual-drum configuration can measure the diameter, speed, and direction of the particle to the accuracy required.

The fiber optic system is most useful when the membranes are held in tension. It is non-contact and responds to out-of-plane displacement, making it well suited for use on very large, thin (2 μm or thicker) films. The data indicate adequate signals would be present using four sensors on a drum as large as 3.5 m diameter, where a drum this size would be needed if the primary focus were on particles larger than 0.5 mm. It is also well suited for identifying modal frequencies and hence, can be used for monitoring film tension and integrity. However, maintaining constant film tension over long periods is a complication unless the system is located in a gravitational field (i.e., lunar surface) or solar wind environment (i.e., solar sail).

For instruments deployed for long periods in free space it would be preferable not to require constant film tension. In this case thicker films instrumented with PVDF sensors are advantageous. They have high sensitivity to in-plane strain and, on these thicker films (i.e., 25 μm), the mechanical loading by the sensor is unimportant. Test data indicate that adequate signals from particles as small as 50 μm in diameter could be obtained using films at least 2 m^2. Larger arrays would require additional sensors or multiple instruments.

These two systems have a longer and richer development history than presented in the short overview here. Various instruments using these sensors have been developed but none of these previous instruments have yet received the priority needed to justify the expense of testing them in space. However, recently a 1-m version of the PVDF system described here has been manifested for a flight to the International Space Station where it will soon begin a 3-yr mission characterizing the MM and debris population at that altitude.

ACKNOWLEDGMENTS

We wish to thank the NASA Orbital Debris Office, and the NASA LASER program for providing support. Also we are indebted to the Science and Technology Facilities Council (UK) for supporting the hypervelocity facility at the University of Kent.

APPENDIX

The multilateration equation derived for this application makes use of two available constraints of our system: the drum surface is planar, and the sensors can be located orthogonally. The number of sensors required is three, which we call *So*, *Sx*, and *Sy*. As illustrated in Fig. 1, sensor location *So* identifies the axis origin (0, 0); sensors *Sx* and *Sy* are along the orthogonal *x*- and *y*-axis at locations (*Lx*, 0) and (0, *Ly*), respectively. (The fourth sensor shown *Sxy* is not used in this derivation.) Data collection start at some arbitrary reference clock-time t_R. The impulsive noise source (i.e., impact) occurs at point (x,y) at some clock-time (t_0+t_R). The acoustic signal from this noise source propagates to the three sensors. The time required to traverse this distance is T_0, T_X, and T_Y, so the signals arrive at clock-times $(T_0+t_0+t_R)$, $(T_X+t_0+t_R)$, and $(T_Y+t_0+t_R)$.

The quantities known are the locations of the sensors, and hence their separation distances *Lx* and *Ly* along the corresponding axes. Also known are the clock-times of the signal arrivals at the sensor. The wave speed c is also treated here as a known, since it is easily measured directly or with the inclusion of a fourth sensor. From the geometry of the system, the three equations describing the arrival times at the sensors are

$$T_0 - t_0 = \frac{1}{c}\sqrt{x^2+y^2}, \tag{A1}$$

$$T_X - t_0 = \frac{1}{c}\sqrt{(L_X-x)^2+y^2}, \tag{A2}$$

$$T_Y - t_0 = \frac{1}{c}\sqrt{x^2+(L_Y-y)^2}, \tag{A3}$$

where by using only time differences after impact any influence of the arbitrary clock start-time reference has been eliminated. These three equations have three unknowns: x, y, and t_0.

We can square these equations and begin reducing them. First, Eq. (A1) can be solved for y^2. This can then be substituted in Eq. (A2) to solve for x:

$$x = \frac{L_X^2 + c^2(T_0-t_0)^2 - c^2(T_X-t_0)^2}{2L_X}. \tag{A4}$$

With the same substitution Eq. (A3) becomes

$$\sqrt{c^2(T_0-t_0)^2 - X^2} = \frac{L_Y^2 + c^2(T_0-t_0)^2 - c^2(T_Y-t_0)^2}{2L_Y}. \tag{A5}$$

As an aside, there is also an analog of Eq. (A4) for y, found using Eqs. (A1) and (A3), which will be useful later in determining the x,y coordinates:

$$y = \frac{L_Y^2 + c^2(T_0-t_0)^2 - c^2(T_Y-t_0)^2}{2L_Y}. \tag{A6}$$

We now have two Eqs. (A4) and (A5) with two unknowns. We can then eliminate x. This provides an equation with only one unknown, t_0. Solving for this results in a very lengthy expression that can be reduced to the following form

$$t_0 = \frac{N + \sqrt{S}}{2D}, \tag{A7}$$

where we label the three terms as D (a denominator term), N (a numerator term), and S (a square-root term). After collecting terms, we simplify the notation by defining two dimensionless parameters:

$$G_X \equiv c^2\left(\frac{T_X - T_0}{L_X}\right), \quad G_Y \equiv c^2\left(\frac{T_Y - T_0}{L_Y}\right)^2. \tag{A8}$$

Then we can eventually arrive at relatively simple expressions for each of the three terms.

$$D = G_X + G_Y - 1, \tag{A9}$$

$$N = G_X(T_X + T_0) + G_Y(T_Y + T_0) - (T_X + T_Y), \tag{A10}$$

$$S = (1 - G_X)(1 - G_Y)\left[\frac{L_X^2 + L_Y^2}{c^2} - (T_X - T_Y)^2\right]. \tag{A11}$$

While this derivation appears exact, there is a limitation. Errors in the measurement of signal arrival time will propagate to an error in location. For example, selecting the dimensions of one of the rectangular films used, we can calculate the location error corresponding to a given error in the signal arrival time. Figure 8 shows a map of the location error resulting from introducing a (large) 10 μs error in the signal arrival time at each of the sensors in turn. The conclusion of such simulations is that the location accuracy is acceptable when the source lies within or near the rectangular area defined by the three orthogonal sensors. However, it fails in the regions immediately behind each sensor location. In principle these regions are described using a negative sign before the square root term of Eq. (A7); in practice using real data, applying this sign change does not reliably improve the results. This issue is also present with other multilateral approaches studied. Fortunately it is of little importance in our application since the region near each sensor will be shielded for other reasons (i.e., to prevent direct impacts from damaging the sensor).

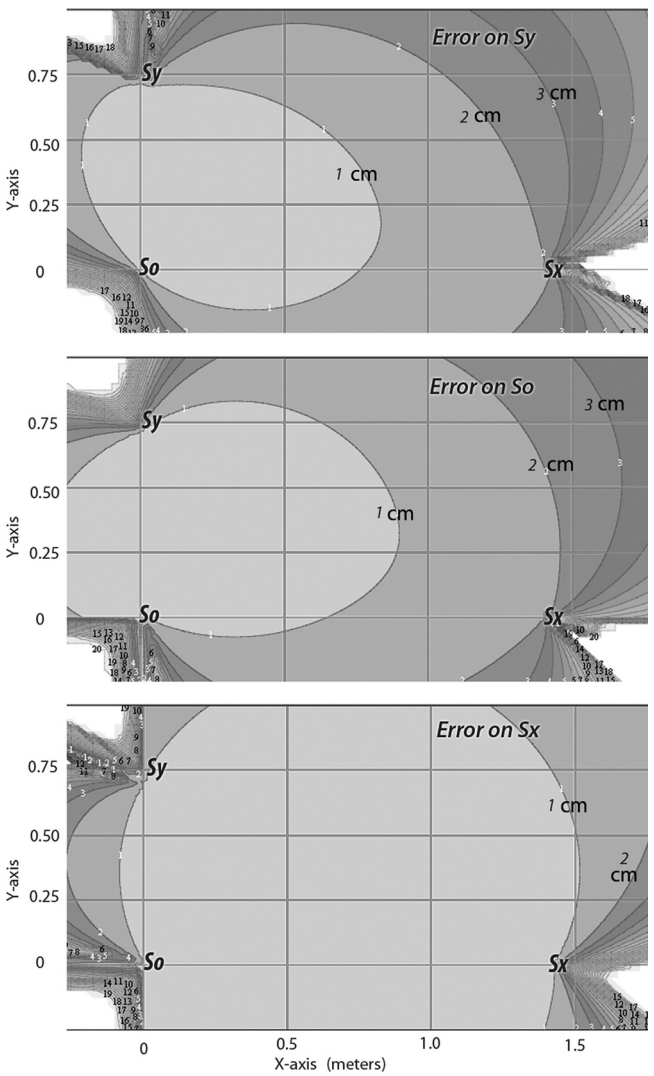

FIG. 8. Example error maps for testing the accuracy of the multilateration approach. The sensor array is 1.5 by 0.75 m. A signal arrival timing error of 10 μs is imposed on one sensor for each case, and the resulting contours correspond to location errors in centimeters.

Bucaro, J. A., Lagakos, N., Houston, B. H., Jarzynski, J., and Zalaludinov, M. (**2005**). "Miniature, high performance, low cost fiber optic microphone," J. Acoust. Soc. Am. **118**, 1406–1413.

Burchell, M. J., Cole, M. J., McDonnell, J. A. M., and Zarnecki, J. C. (**1999a**). "Hypervelocity impact studies using the 2 MV Van de Graaff dust accelerator and two stage light gas gun of the University of Kent at Canterbury," Meas. Sci. Tech. **10**, 41–50.

Burchell, M. J., Thomson, R., and Yano, H. (**1999b**). "Capture of hypervelocity particles in aerogel: In ground laboratory and low Earth orbit," Planet. Space Sci. **47**, 189–204.

Christiansen, E. L. (**2009**). *Handbook for Designing MMOD Protection* (JSC-64399, NASA Publications, Houston, TX), pp. 107–145.

Corsaro, R., Giovane, F., Tsou, P., Liou, J.-C., Buzasi, D., and Gustson, B. (**2004**). "PINDROP – An acoustic particle impact detector," Orbital Debris Q. **8**(3), 3–4, available from NASA archive: http://orbitaldebris.jsc.nasa.gov/newsletter/pdfs/ODQNv8i3.pdf.

Corsaro, R., Liou, J.-C., and Giovane, F. (**2011**). "Spacecraft damage-detection system for human habitation modules," J. Acoust. Soc. Am. **129**(**4**), Pt. 2, 2612. Also highlighted as an ASA 161st Meeting Lay Language Paper.

Corsaro, R., Liou, J.-C., Giovane, F., and Tsou, P. (**2007**). "Continuous large-area micrometeoroid flux measuring instrument," in *Proceedings of Dust in Planetary Systems*, edited by A. Wilson (ESA SP-643, Noordwijk, The Neatherlands), pp. 235–238.

Courbin, L., Marchand, A., Vaziri, A., Ajdari, A., and Stone, H. A. (**2006**). "Impact dynamics for elastic membranes," Phys. Rev. Lett. **97**, 244301.

Duffy, D. G. (**2001**). *Green's Functions with Applications* (Chapman & Hall/CRC, London, UK), pp. 108–110.

Green, S. F., Williams, I. P., McDonnell, J. A. M., and McBride, N. (Eds.) (**2002**). "Dust in the Solar System and other planetary systems," in *COSPAR Colloquia Series* (Elsevier Science Ltd., Oxford, UK), Vol. 15, 426 pp.

Grun, E., Gustafson, B. A. S., Dermott, S. F., and Fechtig, H. (Eds.) (**2001**). *Interplanetary Dust* (Springer-Verlag, New York), 804 pp.

Kearsley, A. T., Graham, G. A., McDonnell, J. A. M., Taylor, E. A., Drolshagen, G., Chater, R. J., McPhail, D., and Burchell, M. J. (**2007**). "The chemical composition of micrometeoroids impacting upon the solar arrays of the Hubble Space Telescope," Adv. Space Res. **39**(4), 590–604.

Lagakos, N., Bucaro, J. A., and Jarzynski, J. (**2012**). "Intensity modulated fiber optic strain sensor," U.S. patent 7646946.

Liou, J.-C. (**2013**). "Micrometeoroid and orbital debris impact inspection of the Hst Wfpc2 radiator," NASA Technical Report 978-1289250836 (July 29, 2013), available from NTRS archive: (http://ntrs.nasa.gov/archive/nasa/casi.ntrs.nasa.gov/20100025563.pdf).

Liou, J.-C., Christiansen, E., Corsaro, R. D., Giovane, F., Tsou, P., and Stansbery, E. (**2005**). "Modeling the meteoroid environment with existing *in situ* measurements and with potential future space experiments," *Proceedings of the Fourth European Conference on Space Debris* (ESA SP-587, Noordwijk, The Neatherlands), pp. 195–200.

Liou, J.-C., Giovane, F., Corsaro, R., and Stansbery, E. (**2007**). "LAD-C: A large area cosmic dust and orbital debris collector on the International Space Station," *Proceedings of Dust in Planetary System* (ESA SP-643, Noordwijk, The Neatherlands), pp. 227–230.

Mckee, M. (**2004**). "Cosmic percussion traces space dust," *New Scientist*, Aug. 28, 2004 (London, UK), p. 20.

Opiela, J. N., Liou, J.-C., Corsaro, R., and Giovane, F. (**2011**). "Demonstration of a particle impact monitoring system for crewed space exploration modules," NASA Technical Report, IAC-11-D5.1.2, pp. 1–7, available from NTRS archive: (http://ntrs.nasa.gov/archive/nasa/casi.ntrs.nasa.gov/20110008306.pdf).

Tuzzolino, A. J., Economou, T. E., McKibben, R. B., Simpson, J. A., BenZvi, S., Blackburn, L., Voss, H. D., and Gursky, H. (**2005**). "Final results from the space dust (SPADUS) instrument flown aboard the Earth-orbiting ARGOS spacecraft," Planet. Space Sci. **53**(9), 903–923.

Tuzzolino, A. J., Economou, T. E., McKibben, R. B., Simpson, J. A., McDonnell, J. A. M., Burchell, M. J., Vaughan, B. A. M., Tsou, P., Hanner, M. S., Clark, B. C., and Brownlee, D. E. (**2003**). "Dust flux monitor instrument for the Stardust mission to comet Wild 2," J. Geophys. Res.: –Planets **108**(E10), 1–24.